MIT Libraries | DSpace@MIT

MIT Open Access Articles

Enhancing the Performance of Viscous Electrode-Based Flow Batteries Using Lubricant-Impregnated Surfaces

The MIT Faculty has made this article openly available. ***Please share*** how this access benefits you. Your story matters.

Citation: Solomon, Brian R. et al. "Enhancing the Performance of Viscous Electrode-Based Flow Batteries Using Lubricant-Impregnated Surfaces." ACS Applied Energy Materials 1, 8 (June 2018): 3614–3621 © 2018 American Chemical Society

As Published: http://dx.doi.org/10.1021/acsaem.8b00241

Publisher: American Chemical Society (ACS)

Persistent URL: https://hdl.handle.net/1721.1/129770

Version: Author's final manuscript: final author's manuscript post peer review, without publisher's formatting or copy editing

Terms of Use: Article is made available in accordance with the publisher's policy and may be subject to US copyright law. Please refer to the publisher's site for terms of use.

Massachusetts Institute of Technology

Enhancing the Performance of Flow Batteries Using Lubricant-Impregnated Surfaces

Brian R. Solomon[a, #], Xinwei Chen[b, #], Leonid Rapoport[a], Ahmed Helal[a], Gareth H. McKinley[a], Yet-Ming Chiang[b,*], Kripa K. Varanasi[a,*]

[a)] Department of Mechanical Engineering [b)] Department of Materials Science and Engineering, Massachusetts Institute of Technology, Cambridge, Massachusetts 02139, United States

[#]Equal contribution

***Corresponding authors' e-mails: varanasi@mit.edu, ychiang@mit.edu**

Abstract

Redox flow batteries are a promising technology that can economically meet the grid storage needs of renewable power sources because they decouple energy and power and provide design flexibility especially at large scales. Today, most redox flow batteries are based on dissolved redox molecules (e.g. vanadium ions) in an aqueous solution and are limited by expensive ion-selective membranes, low active material solubility, and low cell voltages. By contrast, non-aqueous semi-solid flow electrodes can utilize insoluble, high potential materials (e.g. Li-ion compounds) but require adding conductive carbon to the suspension which increases the yield stress of the suspension and thereby the power required to drive flow. For instance, recently a gravity-induced flow battery (GIFcell) was demonstrated, but the design could only flow electrode suspensions with yield stresses <1 Pa and as a result the carbon loading of the lithium-polysulfide (Li-PS) flow electrode was limited to 0.5vol% even when using hydrophobic, flat Teflon surfaces in the flow channels. A modest capacity <200 mAh/g (<12% of the theoretical capacity) was extracted from the flow electrode because only limited carbon loading could be achieved. The present work introduces lubricant-impregnated surfaces (LIS) to promote the flow of paste-like flow electrode materials with >1 Pa yield stress and outlines the design of LIS for flow cells based on interfacial thermodynamics and electrochemical stability. Using a Li-PS flow electrode with 0.75vol% Ketjenblack as the conductive carbon (yield stress of 4 Pa), we demonstrate that LIS can provide as much as 86% power

savings over conventional, non-slipping surfaces at low flow rates (corresponding to a flow rate < 3 mm^3/s for the configuration used). Experimentally, LIS are applied to the GIFcell in a half-flow-cell configuration and a specific capacity of ~800 mAh/g is demonstrated which is a fourfold increase compared to previous work. The Li-PS flow electrode is able to flow continuously without pinning, demonstrating the functionality and stability of the LIS in a flow battery configuration.

Keywords: Electrochemistry, Liquid-Impregnated Surfaces, Flow Batteries, Slip, Yield Stress, Drag Reduction

1. Introduction

Integrating renewable power sources such as solar and wind with the electric grid[1] can reduce the reliance on fossil fuel which is a diminishing natural resource.[2] Large-scale energy storage is required to overcome the intermittency of these sources to ensure reliability in providing electricity to meet demand.[3–11] Redox flow batteries (**Figure 1**a) that are driven by pumps or gravity are a promising technology for large-scale energy storage due to their potential to meet the cost target of ~$100 per kWh at a system level and their ease of scalability.[12,13] Today, most redox flow batteries are based on flowable electrodes comprising dissolved redox molecules (e.g. vanadium ions) in an aqueous solution. However, expensive ion-selective membranes, low solubility of active materials (<2 M), and low cell voltages of <1.2 V (limited by the electrolysis of water) challenge widespread commercialization.

Flow electrodes based on semi-solid suspensions,[13–27] on the other hand, can increase the energy density of redox flow batteries by an order of magnitude by using lithium intercalation compounds.[14] A continuous percolating network of nano-scale carbon (such as Ketjenblack ECP600JD) provides electronic conductivity to the suspended active materials in the electrolyte. Higher loadings of carbon in the flow electrode allow for higher current densities and lower polarization but drastically increase the yield stress of the flow electrode.[13] For example when discharged at a rate of C/5 (corresponding to a discharge current that would discharge the entire battery capacity in five hours), increasing the carbon content from 0.50 to 0.75vol% for flow electrodes comprising 2.5 M sulfur more than doubles the conductivity (Figure 1b) and increases the capacity threefold from ~250 to ~750 mAh/g (Figure 1c). The effective increase in capacity at higher loadings, however, has the adverse effect of increasing the yield stress as shown in Figure 1b, in which increasing the carbon content from 0.50 to 0.75vol% increases the yield stress from 1.3 to 4 Pa (see Figure S3 and Table S1 for complete rheology).

Slippery surfaces can potentially allow the flow of electrodes comprising higher carbon loadings by decreasing the viscous dissipation at the walls to realize effective capacity gains. Furthermore, enhancing wall slip in semi-solid flow cells promotes plug-like flow and improves both mechanical and energetic efficiencies[28] while avoiding

conductivity loses associated with induced disruption of the carbon network.[19,29] In the present paper, lubricant-impregnated surfaces (LIS, depicted in **Figure 2**a) are designed to promote the flow of suspensions for electrochemical systems. A canonical LIS is composed of a liquid lubricant that is stabilized in a porous or textured solid by capillary forces.[30–34] Sessile drops can exhibit high mobility and remarkably low contact angle hysteresis (<1˚) on a stable LIS. In fact, LIS can outperform certain superhydrophobic surfaces in applications including reducing drag for internal flows of Newtonian liquids.[35–37] Herein, we demonstrate that LIS can be applied to the design of flow batteries with electrodes comprising a wide variety of solvents. In particular, we explore using LIS to enable the flow of a lithium polysulfide flow electrode (Li-PS)[13,22] comprising 2.5 M sulfur in triglyme where conductivity is imparted by 0.75vol% of dispersed Ketjenblack (KB) and 0.5 M LiTFSI (lithium bis(trifluoromethanesulfonyl)imide) and 1wt% $LiNO_3$ are also added as the supporting salt and solid electrolyte interphase additive respectively (see Experimental Procedures).

2. Lubricant-impregnated surfaces (LIS)

Figure 2a depicts an LIS in which a liquid lubricant impregnates a porous or textured solid. In order to design LIS for use in an electrochemical system: (1) the lubricant should be immiscible with the working fluid, (2) the lubricant must be electrochemically inactive, and (3) the lubricant must preferentially wet the porous walls in the presence of the working fluid.

In order to function as designed, the lubricant and the working fluid (in this case the flow electrode) should be immiscible; otherwise, no interface would exist. Flow electrode solvents demonstrated in the literature are diverse[12] and a suitable lubricant should be immiscible with all common solvents to simplify the battery design. Both silicone oils and fluorinated liquids are appropriate choices due to their stability and widespread manufacture. These oils have been screened for miscibility with nine commons solvents. Whereas the fluorinated liquids are immiscible with all solvents, silicone oil was found to be miscible with several including dichloromethane, diglyme, and THF . The results for all solvents are presented in Table S2.

Additionally the lubricant must be electrochemically stable and have been screened for electrochemical activity in the voltage window of the cell's operation. Consistent with the electrochemical cycling described later in this paper, lubricants are screened for electrochemical activity in a voltage window of 1.6 to 2.8 V with respect to Li/Li^+. Figure 2b, c shows the cyclic voltammogram of several fluorinated liquids and silicone oil as well as a solvent triglyme for references. The current densities (<1.5 $\mu A/cm^2$) over the voltage window are significantly less than typical electrochemical reactions (>0.1 mA/cm^2), hence all the fluorinated liquids and silicone oil are electrochemically inactive.

Finally, the lubricants need to be thermodynamically stable to form an LIS. As depicted in Figure 2a, a working fluid in contact with a porous solid and lubricant can form three distinct morphologies. The encapsulated state is characterized by the lubricant encapsulating the solid including spreading everywhere between the solid and working fluid. This state maximizes the mobility of the working fluid.[34] In contrast, the working fluid may preferentially wet the solid and displace the lubricant to form an impaled state that increases the friction and reduces the mobility. In the emerged state, lubricant fills the porous solid but does not spread completely between the solid and working fluid.

Interfacial energies of the system determine which of these three states are favored thermodynamically. In the following discussion:

- Interfacial energies are denoted by γ_{ow}, γ_{os}, and γ_{ws} for the lubricant-working fluid, lubricant-solid, and working fluid-solid interfaces respectively.
- The fraction of solid that is not covered by the lubricant is denoted by ϕ.
- The total surface area of the solid divided by its projected area is the Wenzel roughness r.

The total interfacial energy per unit projected area of each state can be written in terms of the interfacial energies and geometric parameters:
For the encapsulated state,

$$E_1 = \gamma_{ow} + r\gamma_{os} \tag{1}$$

For the emerged state,

$$E_2 = (1-\phi)\gamma_{ow} + (r-\phi)\gamma_{os} + \phi\gamma_{ws} \tag{2}$$

For the impaled state,

$$E_3 = r\gamma_{ws} \tag{3}$$

It is useful to rewrite the above conditions by introducing the spreading coefficient of the lubricant on the solid in the presence of the working fluid denoted as:

$$S_{ow(s)} = \gamma_{ws} - \gamma_{ow} - \gamma_{os} \tag{4}$$

In particular, the spreading coefficient $S_{ow(s)}$ contains no geometrical parameters and is a function of the three interfacial energies. The lubricant will spread and fully wet the solid in the presence of the working fluid only if $S_{ow(s)} > 0$. Rewriting the conditions presented above in terms of the spreading parameter gives:

For the encapsulated state,

$$E_1 < E_2 \tag{5}$$

$$E_3 \geq S_{ow(s)} > 0 \tag{6}$$

For the emerged state,

$$E_2 < E_1 \tag{7}$$

$$E_3 \geq -\gamma_{ow}(r-1)(r-\phi)^{-1} < S_{ow(s)} < 0 \tag{8}$$

For the impaled state,

$$E_3 < E_1 \tag{9}$$

$$E_2 \geq S_{ow(s)} < -\gamma_{ow}(r-1)(r-\phi)^{-1} \tag{10}$$

As shown earlier, fluorinated liquids are immiscible to a wider range of solvents than silicone oils and are also electrochemically inactive. To create an LIS suitable for a flow battery, a fluorinated liquid (Krytox) is chosen as the lubricant and a porous Teflon is chosen as the textured solid due to its chemical similarly to fluorinated liquids. The

Krytox/Teflon LIS is validated for nine common solvents used in flow batteries (surface tensions γ_w = 25 - 72 mN/m): acetonitrile, dichloromethane, diglyme, dimethyl sulfoxide (DMSO), polypropylene carbonate (PC), tetraethylene glycol dimethyl ether (TEG-DME), tetrahydrofuran (THF), triglyme, and water. Porous Teflon samples are stably impregnated with Krytox (see Experimental Procedures) and submerged in each solvent for five days. The sample is then removed and a 5 μL drop of solvent is placed on the surface. In all cases, the solvent drop rolls from the sample when it is tilted to <5˚ indicating that the Krytox/Teflon LIS retain their slippery properties and are stable in all solvents (Supporting Video S4).

To quantify the interaction between the flow electrode and surface, a torsional rheometer with a parallel plate geometry is used. By taking measurements at multiple gaps (Figure S3), the method proposed by Yoshimura & Prud'homme[38] can quantify the slip velocity u_s as a function of the applied shear stress τ (see Experimental Procedures). The results are presented in **Figure 3**a for the lithium polysulfide suspension on three different surfaces. A stainless steel surface sputtered with gold is used as the control and shows no-slip, and a Teflon surface is used for comparison. For both the LIS and Teflon a critical slip model[39] is used:

$$u_s = 0 \quad \text{for} \quad \tau < \tau_c \tag{11}$$

$$u_s = \beta(\tau - \tau_c) \quad \text{for} \quad \tau \geq \tau_c \tag{12}$$

where τ_c is the critical shear stress required for the onset of slip and β is the slip coefficient. A fit to the experimental data of Figure 3a gives τ_c = 0.57 Pa and β = 87 μm·Pa^{-1}·s^{-1} for flow on LIS (R^2 = 0.99) and τ_c = 1.26 Pa and β = 68 μm·Pa^{-1}·s^{-1} for flow on Teflon (R^2 = 0.998). For a given stress, LIS has a higher slip velocity than Teflon.

In order to predict the effects of slip in a flow, results from the slip analysis are used to compute the laminar flow of a pressure-driven flow in a rectangular channel. The steady Cauchy momentum equation is solved using the Bingham model and critical slip model for a channel that is 10 mm wide, 1 mm in height, and 200 mm long. The details of this calculation are presented in the Supporting Information.

The flow rate for a given applied pressure is presented in Figure 3b for the cases when the channel walls are no-slip, flat Teflon, and LIS. On the no-slip surface, there is

no flow until the yield stress of the material is overcome at around 1.65 kPa (see Supporting Information). When the channel is comprised of LIS or flat Teflon however, plug flow occurs once the critical stress for the onset of slip is overcome. The asterisks on the plots indicate the point at which the flow begins to yield. For flow on LIS and flat Teflon, Li-PS flows entirely as a plug up to a driving pressure of 1.65 kPa.

The mechanical power $\dot{W}$ required to drive the flow cell is the product of the flow rate and pressure drop and is presented in Figure 3c. Figure 3d provides a direct comparison of the three different surfaces in the flow channel where the mechanical power savings of surface A over surface B is calculated as $1-\dot{W}_A/\dot{W}_B$. At low flow rates, LIS provide an 86% mechanical power savings over a no-slip surface and flat Teflon provides 70% power savings.

Before yielding, all of the power dissipation occurs at the walls of the flow channel. After yielding, the dissipation is the result of a combination of slip at the wall and shear in the bulk suspension. The latter contribution becomes increasingly more important at higher flow rate (see Supporting Information) and as a result the mechanical power savings should decrease at high flow rates.

Figure 4 visually demonstrates the ability of LIS to promote slip. In Figure 4a a drop of Li-PS suspension (yield stress σ_y = 4 Pa) placed on a gold surface flows under gravity but shortly thereafter stops flowing and the trailing edge remains pinned on the substrate. The same drop, however, slides on the LIS (Figure 4b). Flat gold is used as a comparison because it is a non-slipping surface (Figure S4). This experiment also highlights the difficulty of overcoming contact line pinning in such a flow and similar results are seen with Teflon (Figure S5). Although low energy materials such as Teflon have been shown to provide slip for yield stress fluids,[40] pinning forces arising from surface roughness limit their effectiveness.[41,42]

Compared to a conventional surface and Teflon, LIS can eliminate pinning and minimize interfacial friction, thus enhancing electrochemical performance (Supporting Videos S1 and S2). The LIS is composed of a porous Teflon membrane impregnated with Krytox 1506 (see Experimental Procedures). In addition, Supporting Video S3 compares the flow in channels made of acrylic to channels lined with LIS where similarly the LIS enables flow.

3. LIS demonstrated in a gravity-induced flow cell

Experimentally, LIS are incorporated into a gravity-induced flow cell (GIFcell),[13] a simple construction with no moving parts that uses energy-dense electrodes that flow under the force of gravity through a centrally positioned electrochemical stack. The LIS can also be integrated into other redox flow battery configurations and chemistries using the same methodology. **Figure 5**a shows a half-cell-flowing GIFcell where the positive flowing electrode and the stationary negative electrode are separated by a porous membrane. Similar to earlier work using the GIFcell,[13] lithium-sulfur chemistry is utilized in the present work in which the positive flowing electrode is a suspension of lithium polysufide (Li-PS) comprising Li_2S_8 (2.5 M with respect to S) in triglyme with 0.75vol% KB (for electronic conductivity), 0.5 M LiTFS (lithium bis(trifluoromethanesulfonyl)imide, for ionic conductivity), and 1wt% $LiNO_3$ (as a solid electrolyte interphase additive). The negative electrode is a stationary lithium metal foil. A Tonen microporous separator (Tonen Chemical Corporation, Japan), with pore sizes smaller than the KB particles, ensures no electrical shorting between the electrodes. An exploded view of the device is included in Figure S6 where LIS line the flow channel except in the current collect region. Figure 5b and Supporting Video S5 show that the Li-PS flowing the GIFCell.

The system is tested in an intermittent-flow mode wherein an aliquot of Li-PS remains stationary during electrochemical cycling.[28] Upon completion of the cycle, the next aliquot flows into the electrochemical active region by tilting the GIFcell as depicted in Figure 5a. The electrochemical energy efficiency for each cycle is calculated as:

$$\text{Energy efficiency} = \frac{V_D I_D t_D}{V_C I_C t_C} \tag{13}$$

where V is the potentiostatic voltage, and It is the total charge delivered. The subscripts D and C represent discharging and charging respectively. Figure 5c shows the potentiostatic cycling performance and Figure 5d shows the discharged capacity and energy efficiency for various aliquots and cycle numbers of the GIFcell with LIS. An energy efficiency of

93% is achieved for the first cycle, which shows that energy can be effectively transferred in and out of the GIFcell. The current density of 0.65-0.7 mA/cm^2 for the first 6 min corresponds to a theoretical C-rate of 1/20 h^{-1}. The current density then decays to 0.2 mA/cm^2, giving a discharge specific density of 777 mAh/g over the duration of 20 hours. This lower current density indicates the presence of low order Li-PS (Li_2S_2 and Li_2S). In the second cycle, a higher average current density of 1.1 mA/cm^2 is obtained for the first 6 min, corresponding to a theoretical C-rate of 1/12 h^{-1}. We hypothesize that this higher current density is due to presence of sulfur species at the start of the discharge, Li_2S_8 vs. Li in the first cycle and S_8 vs. Li in the second cycle, resulting in a higher overpotential. The second aliquot is then moved into the active region by tilting the GIFcell in which about 770 mAh/g of capacity is extracted.

4. Outlook

Flow electrodes based on semi-solid suspensions expand the material design space for flow batteries beyond traditional dissolved redox molecules and allow the use of more energy dense materials. Inevitably however, these semi-solid suspensions exhibit yield stress behavior due to the necessary incorporation of carbon to impart electronic conductivity and are consequently challenging to flow. Low surface energy materials such as Teflon are not sufficient to allow repeatable flow as they do not eliminate pinning forces. The present work successfully demonstrates the use of LIS in an electrochemical system to introduce robust and repeatable slip and to enable the flow of an otherwise non-flowing lithium polysulfide electrode in a GIFcell.

In future works, additional benefits from incorporating LIS into flow batteries can be demonstrated including boosting energetic efficiencies resulting from a modified velocity profile due to slip[28] and mitigating conductivity losses associated with shearing of the carbon network.[19,29] In addition, the design rules laid out here for incorporating LIS into batteries and previous work demonstrating inhibition of mineral scale formation in aqueous systems[43] can be developed to mitigate precipitate formation in both flowing and non-flowing battery configurations.

Experimental Procedures

All electrochemical and rheological testing was conducted in an Argon-filled glove box (MBRAUN, Newburyport, MA, US) with oxygen and moisture levels maintained below 5 and 1 ppm, respectively.

The lithium polysulfide flow electrode was formulated by adding 1 wt% of lithium nitrate ($LiNO_3$, Sigma-Aldrich) and 0.5 M of lithium bis(trifluoromethanesulfonyl)imide (LiTFSI, Sigma-Aldrich) to triglyme (Sigma-Aldrich). Lithium sulfide (Li_2S, Alfa) and sulfur (Sigma-Aldrich) was then added to the solution to a total sulfur concentration of 2.5 M. The mixture was stirred mechanically at a temperature of 60°C for 12 h to obtain a dark brown lithium polysulfide (Li_2S_8) solution. Conductive carbon black (Ketjenblack ECP600JD, Azko Nobel Polymer Chemicals LLC, Chicago, Illinois, US) was combined with half of the Li_2S_8 solution in a 20 mL glass vial and then the rest of the Li_2S_8 solution was added. This method of mixing was found to yield a more reproducible suspension compared to directly adding the KB to the solution. The resulting suspension was then sealed in a vial by black insulating tape and removed from the glove box. The vial was sonicated in an ultrasonic bath for 60 min to obtain homogeneity before testing.

To create the LIS, a Teflon membrane (PTFE Unlaminated Membrane Filters, Sterlitech Corporation, United States) with an effective pore size of either 200 nm or 1 μm pores was lowered perpendicularly into a bath of Krytox 1506 (DuPont) at 10 mm/min to prevent air bubbles from becoming trapped on the surface. In all experiments, the membranes with effective pore size of 200 nm were used. When withdrawing the membrane above a critical capillary number Ca_C, an excess film is viscously entrained. During battery operation, such an excess film would be dragged by the flowing electrolyte and compromise conductivity. For capillary numbers $Ca_C = \mu_0 V_{crit}/\gamma < 10^{-4}$, no excess film is viscously entrained.[44] Here, μ_0 is the viscosity of the lubricant (117 cP), γ is its surface tension (17 mN/m), and V_{crit} is the critical withdrawal speed. In order to prevent an excess film, the Teflon membrane was withdrawn from a bath of Krytox lubricant below V_{crit} at a rate of 2 mm/min. The resulting liquid-impregnated surfaces (LIS) were then lightly rinsed with isopropyl alcohol.

Rheology was measured using a Malvern Kinexus Pro torsional rheometer enclosed in a glove box. Steady shear viscometry tests were performed using a smooth

parallel plate geometry (40 mm diameter, mean roughness 0.36 μm). For tests using the Teflon and LIS surfaces, the test surface was applied to both the top and bottom plates. All tests were performed at 25 °C, which was regulated with a Peltier plate system. All samples were pre-sheared at 100 s^{-1} prior to measurement and left to equilibrate until the normal force has relaxed (~15 min). Steady shear tests were performed with decreasing applied shear rates as described by Ovarlez et al.[45] to insure the yield stress of the material is reached and to avoid possible transient shear banding. In addition, following the protocol proposed by Yoshimura & Prud'Homme,[38] the same sample was tested at three different gaps (660, 500, and 400 μm) to probe and correct for slip effects (Figure S4). If the flow curves at different gap heights superimpose, the material does not slip. If gap-dependent rheology is observed, a correction needs to be applied to extract the true shear rate applied on the sample at each value of the applied stress. The apparent shear rate $\dot{\gamma}_a(\tau)$ can be written in terms of the true shear rate $\dot{\gamma}(\tau)$, the slip velocity $u_s(\tau)$ and the gap H:

$$\dot{\gamma}_a(\tau) = \dot{\gamma}(\tau) + \frac{2u_s(\tau)}{H} \tag{14}$$

For each stress, the apparent shear rate is plotted against $1/H$ to deduce the slip velocity $u_s(\tau)$.[38]

For cyclic voltammetry tests to measure the electrochemical stability of lubricants, Swagelok® type cells with 0.56 mm deep and 0.55 mm diameter circular wells were used. Lithium was used as the counter and reference electrode. A Tonen separator (Tonen Chemical Corporation, Japan) soaked with the electrolyte (0.5 M LiTFSI, 1wt% $LiNO_3$ in triglyme) separated the lithium from the cathode. The cathode consisted of 5 μL of the solution of interest. The voltage was swept between 1.6 and 2.8 V with respect to Li/Li+, at a 10 mV/s scan rate. All cell assembly was performed inside an argon-filled glovebox. The cells were tested on a Solartron potentiostat operating a 1400 Cell Test System.

Prior to assembly of the GIFcell, the following procedures were carried out. The stainless steel current collector that would be in contact with the cathode material was sputtered with gold to reduce interfacial impedance. The LIS were placed on the flow

channels. The GIFcell parts were then assembled in the glove box. A thin foil of lithium was placed on a current collector and wrapped with a Tonen separator soaked with the electrolyte (0.5 M LiTFSI, 1wt% $LiNO_3$ in triglyme) separated the lithium from the cathode. The wrapped current collector was then secured in place. The two plates of the GIFcell were secured using bolts and nuts. The flow electrode (Li_2S_8 suspension) was introduced into one side of the channel by injection with a syringe through a port. The GIFcell was tested on a Solartron potentiostat operating a 1400 Cell Test System.

Acknowledgements

This work was supported as part of the Joint Center for Energy Storage Research, an Energy Innovation Hub funded by the U.S. Department of Energy, Office of Science, Basic Energy Sciences. BRS acknowledges financial support from the Martin Family Society of Fellows for Sustainability. XC acknowledges financial support from the Agency for Science, Technology and Research (A*STAR), Singapore.

References

[1] H. Lund, *Energy* **2007**, *32*, 912.
[2] S. Shafiee, E. Topal, *Energy Policy* **2009**, *37*, 181.
[3] R. M. Dell, D. A. J. Rand, *J. Power Sources* **2001**, *100*, 2.
[4] B. Dunn, H. Kamath, J.-M. Tarascon, *Science* **2011**, *334*, 928.
[5] H. Ibrahim, A. Ilinca, J. Perron, *Renew. Sustain. Energy Rev.* **2008**, *12*, 1221.
[6] B. Dunn, H. Kamath, J.-M. Tarascon, *Science* **2011**, *334*, 928.
[7] P. G. Bruce, S. A. Freunberger, L. J. Hardwick, J.-M. Tarascon, *Nat. Mater.* **2012**, *11*, 19.
[8] W. Wang, Q. Luo, B. Li, X. Wei, L. Li, Z. Yang, *Adv. Funct. Mater.* **2013**, *23*, 970.
[9] R. Van Noorden, *Nature* **2014**, *507*, 26.
[10] D. Larcher, J.-M. Tarascon, *Nat. Chem.* **2015**, *7*, 19.
[11] J. W. Choi, D. Aurbach, *Nat. Rev. Mater.* **2016**, *1*, 16013.
[12] A. Z. Weber, M. M. Mench, J. P. Meyers, P. N. Ross, J. T. Gostick, Q. Liu, *J. Appl. Electrochem.* **2011**, *41*, 1137.
[13] X. Chen, B. J. Hopkins, A. Helal, F. Y. Fan, K. C. Smith, Z. Li, A. H. Slocum, G. H. McKinley, W. C. Carter, Y.-M. Chiang, *Energy Environ. Sci.* **2016**, *9*, 1760.
[14] M. Duduta, B. Ho, V. C. Wood, P. Limthongkul, V. E. Brunini, W. C. Carter, Y.-M. Chiang, *Adv. Energy Mater.* **2011**, *1*, 511.
[15] F. R. Brushett, J. T. Vaughey, A. N. Jansen, *Adv. Energy Mater.* **2012**, *2*, 1390.
[16] Z. Li, K. C. Smith, Y. Dong, N. Baram, F. Y. Fan, J. Xie, P. Limthongkul, W. C. Carter, Y.-M. Chiang, *Phys. Chem. Chem. Phys.* **2013**, *15*, 15833.
[17] S. Hamelet, D. Larcher, L. Dupont, J.-M. Tarascon, *J. Electrochem. Soc.* **2013**, *160*, A516.
[18] Q. Lai, H. Zhang, X. Li, L. Zhang, Y. Cheng, *J. Power Sources* **2013**, *235*, 1.
[19] M. Youssry, L. Madec, P. Soudan, M. Cerbelaud, D. Guyomard, B. Lestriez, *Phys. Chem. Chem. Phys.* **2013**, *15*, 14476.
[20] Y. Yang, J. Loomis, H. Ghasemi, S. W. Lee, Y. J. Wang, Y. Cui, G. Chen, *Nano Lett.* **2014**, *14*, 6578.
[21] K. B. Hatzell, L. Fan, M. Beidaghi, M. Boota, E. Pomerantseva, E. C. Kumbur, Y. Gogotsi, *ACS Appl. Mater. Interfaces* **2014**, *6*, 8886.
[22] F. Y. Fan, W. H. Woodford, Z. Li, N. Baram, K. C. Smith, A. Helal, G. H. McKinley, W. C. Carter, Y.-M. Chiang, *Nano Lett.* **2014**, *14*, 2210.
[23] K. B. Hatzell, M. Boota, E. C. Kumbur, Y. Gogotsia, *J. Electrochem. Soc.* **2015**, *162*, A5007.
[24] X. Wei, L. Cosimbescu, W. Xu, J. Z. Hu, M. Vijayakumar, J. Feng, M. Y. Hu, X. Deng, J. Xiao, J. Liu, V. Sprenkle, W. Wang, *Adv. Energy Mater.* **2015**, *5*, DOI 10.1002/aenm.201400678.
[25] H. Chen, Q. Zou, Z. Liang, H. Liu, Q. Li, Y.-C. Lu, *Nat. Commun.* **2015**, *6*, 5877.
[26] S. Zhang, K. Ueno, K. Dokko, M. Watanabe, *Adv. Energy Mater.* **2015**, *5*, n/a.
[27] K. B. Hatzell, M. Boota, Y. Gogotsi, *Chem. Soc. Rev.* **2015**, *44*, 8664.
[28] K. C. Smith, Y.-M. Chiang, W. C. Carter, *J. Electrochem. Soc.* **2014**, *161*, A486.
[29] A. Helal, T. Divoux, G. H. McKinley, *Phys. Rev. Appl.* **2016**, *6*, 64004.
[30] D. Quéré, *Rep. Prog. Phys.* **2005**, *68*, 2495.

[31] J. D. Smith, R. Dhiman, K. Varanasi, *64th Annu. Meet. APS Div. Fluid Dyn.* **2011**, *56*, S4.00001.
[32] T.-S. Wong, S. H. Kang, S. K. Y. Tang, E. J. Smythe, B. D. Hatton, A. Grinthal, J. Aizenberg, *Nature* **2011**, *477*, 443.
[33] A. Lafuma, D. Quéré, *EPL Europhys. Lett.* **2011**, *96*, 56001.
[34] J. D. Smith, R. Dhiman, S. Anand, E. Reza-Garduno, R. E. Cohen, G. H. McKinley, K. K. Varanasi, *Soft Matter* **2013**, *9*, 1772.
[35] B. R. Solomon, K. S. Khalil, K. K. Varanasi, *Langmuir* **2014**, *30*, 10970.
[36] C. Schönecker, S. Hardt, *Microfluid. Nanofluidics* **2015**, 1.
[37] A. A. Hemeda, H. V. Tafreshi, *Langmuir* **2016**, DOI 10.1021/acs.langmuir.5b04754.
[38] A. Yoshimura, R. K. Prud'homme, *J. Rheol.* **1988**, *32*, 53.
[39] S. H. Anastasiadis, S. G. Hatzikiriakos, *J. Rheol.* **1998**, *42*, 795.
[40] S. G. Hatzikiriakos, *Soft Matter* **2015**, *11*, 7851.
[41] S. P. Meeker, R. T. Bonnecaze, M. Cloitre, *Phys. Rev. Lett.* **2004**, *92*, 198302.
[42] O. Merkak, L. Jossic, A. Magnin, *J. Non-Newton. Fluid Mech.* **2006**, *133*, 99.
[43] S. B. Subramanyam, G. Azimi, K. K. Varanasi, *Adv. Mater. Interfaces* **2014**, *1*, 1300068.
[44] J. Seiwert, C. Clanet, D. Quéré, *J. Fluid Mech.* **2011**, *669*, 55.
[45] G. Ovarlez, K. Krishan, J. Goyon, P. Coussot, *J. Non-Newton. Fluid Mech.* **2013**, *193*, 68.

Figures

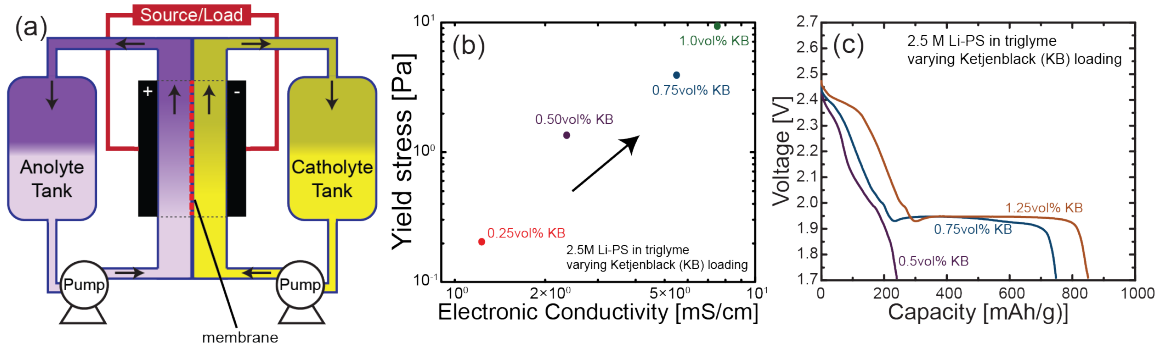

Figure 1: (a) Schematic diagram of a conventional redox flow battery, which consists of two fluid tanks, from which the cathode and anode flow through an electrochemical cell stack. (b) Relationship between the yield stress and electronic conductivity for Li-PS suspensions as a function of Ketjenblack (KB) loading. (c) The Li-Li_2S_8 reaction during the 2nd galvanostatic cycle in a Swagelok cell type configuration at a C/5 rate shows an increasing dependency on the Ketjenblack (KB) loading in the catholyte suspension. The catholyte is comprised of 2.5 M Li-PS with varying concentrations and is 560 µm thick.

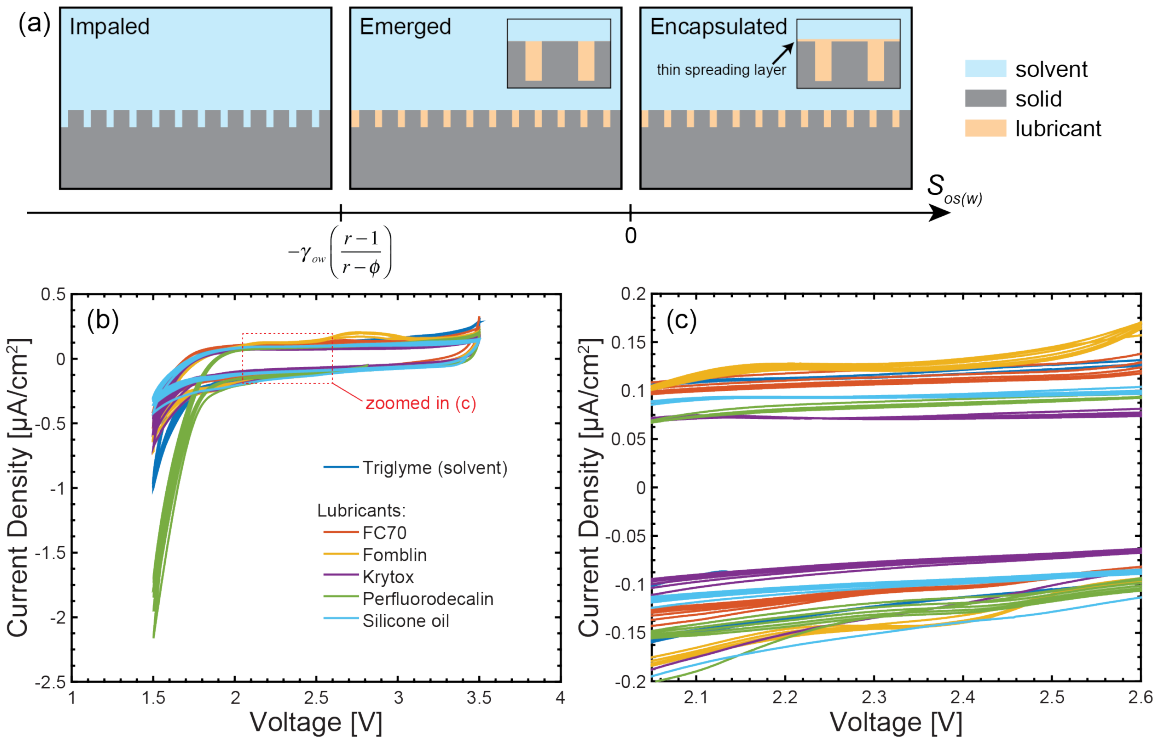

Figure 2: (a) Schematic of an LIS in which a liquid lubricant is stabilized in a porous or textured solid and can exhibit one of three distinct morphologies as determined by the spreading coefficient $S_{os(w)}$ of the lubricant (o) on the solid (s) in the presence of working fluid (w) as indicated on the axis. When $S_{os(w)} > 0$ the lubricant completely spreads over the solid and when $S_{os(w)} < 0$ the LIS can either be unstable (such that the solvent becomes impaled) or form an LIS where the tops of the solid features aren't covered by lubricant. The insets highlight that in the encapsulated state a thin layer of lubricant covered the tops of solid features. (b) Cyclic voltammogram of several candidate lubricants and triglyme conducted at a scan rate of 10 mV/s. Lithium is used as the counter and reference electrodes. A Tonen separator wetted with the electrolyte is used in all the tests. (c) Zoomed region depicted in (b) showing a current density ~0.1 μA/cm^2 for the lubricants and solvent. The current expected in an electrochemical cell is more than two orders of magnitude greater.

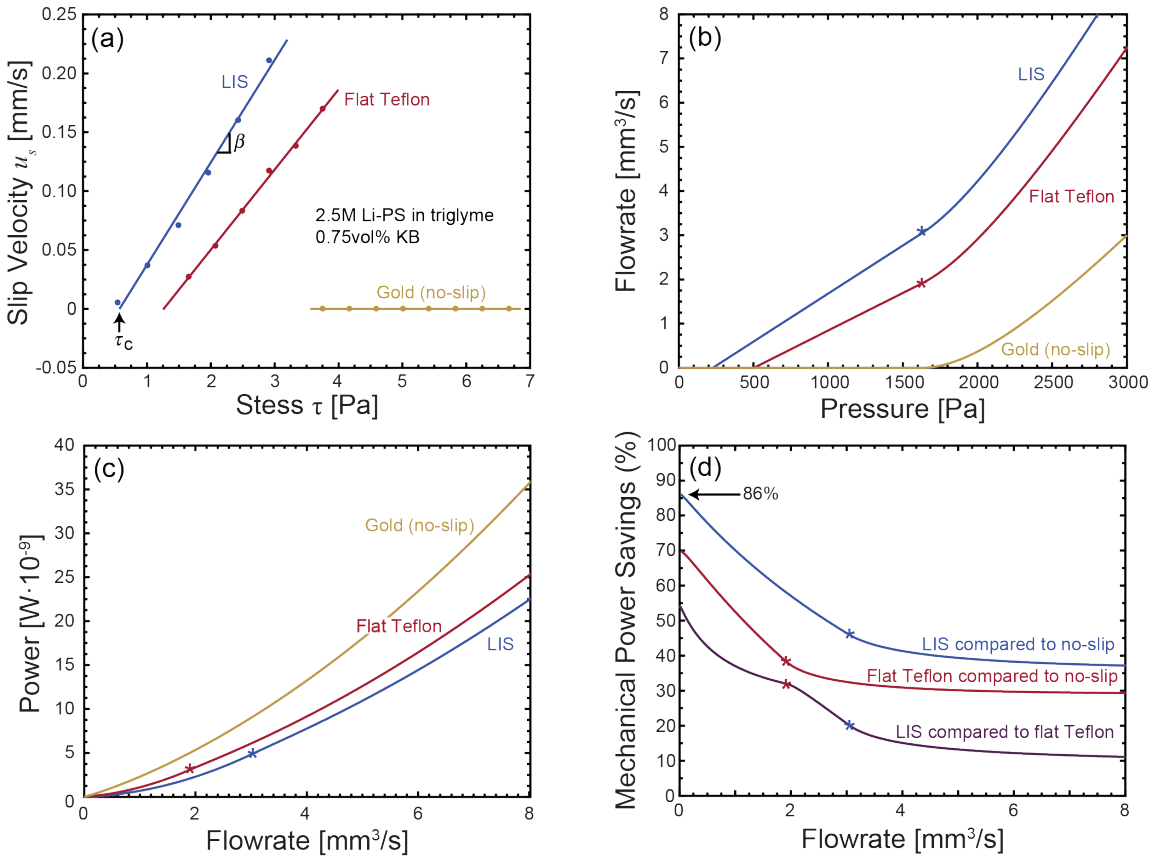

Figure 3: (a) Slip velocity vs. stress for the flow of a 2.5M Li-PS suspension with 0.75vol% KB on LIS, a flat Teflon surface, and a gold surface with linear fits $u_s = \beta(\tau - \tau_c)$ where τ_c is the critical stress for the onset of slip and β the slip coefficient. Because the critical stress τ_c is lower for LIS as compared to flat Teflon, the Li-PS suspension slips more easily on LIS as compared to Teflon. (b) Computed flow rate vs. driving pressure for the same suspension in a 1 x 10 mm rectangular channel that is 20 cm long, (c) Computed power vs. flow rate for the same parameters in (b). On the no-slip surface, there is no flow until the yield stress of the material is overcome at around 1.65 kPa. When the channel is comprised of LIS or flat Teflon however, plug flow happens at lower pressures once the critical stress for the onset of slip is overcome. The asterisk on the plot indicates the point at which the flow begins to yield. For flow on LIS and flat Teflon, Li-PS flow entirely as a plug until 1.65 kPa. (d) Power savings percentage comparing the three surfaces (see Supporting Information).

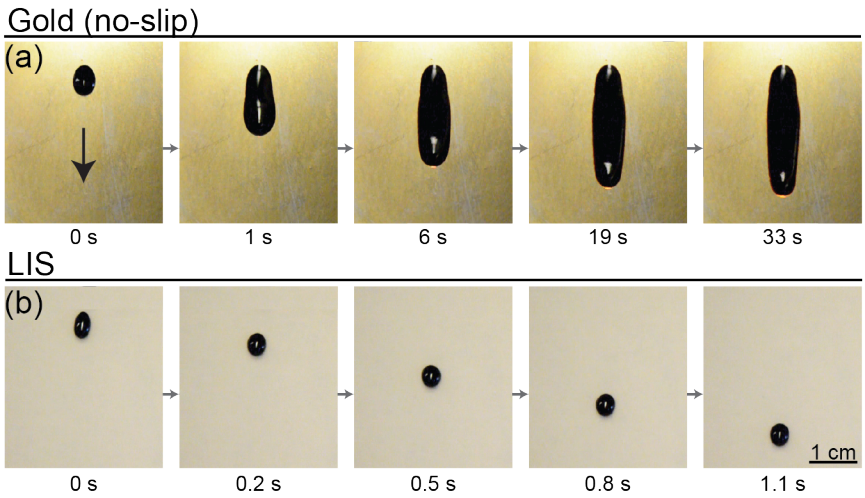

Figure 4: Time-lapse from Supporting Video S1 comparing the flow behavior of a 2.5 M Li-PS suspension with 0.75vol% KB on (a) flat gold surface tilted to 60˚ and (c) an LIS tilted to 60˚. The flow electrode drop yields under gravity on gold but shortly thereafter stops flowing, and the trailing edge remains pinned on the substrate. The same drop, however, slides on the LIS. Flat gold is used as a non-slip surface (Figure S4). Both drops are 25 µL.

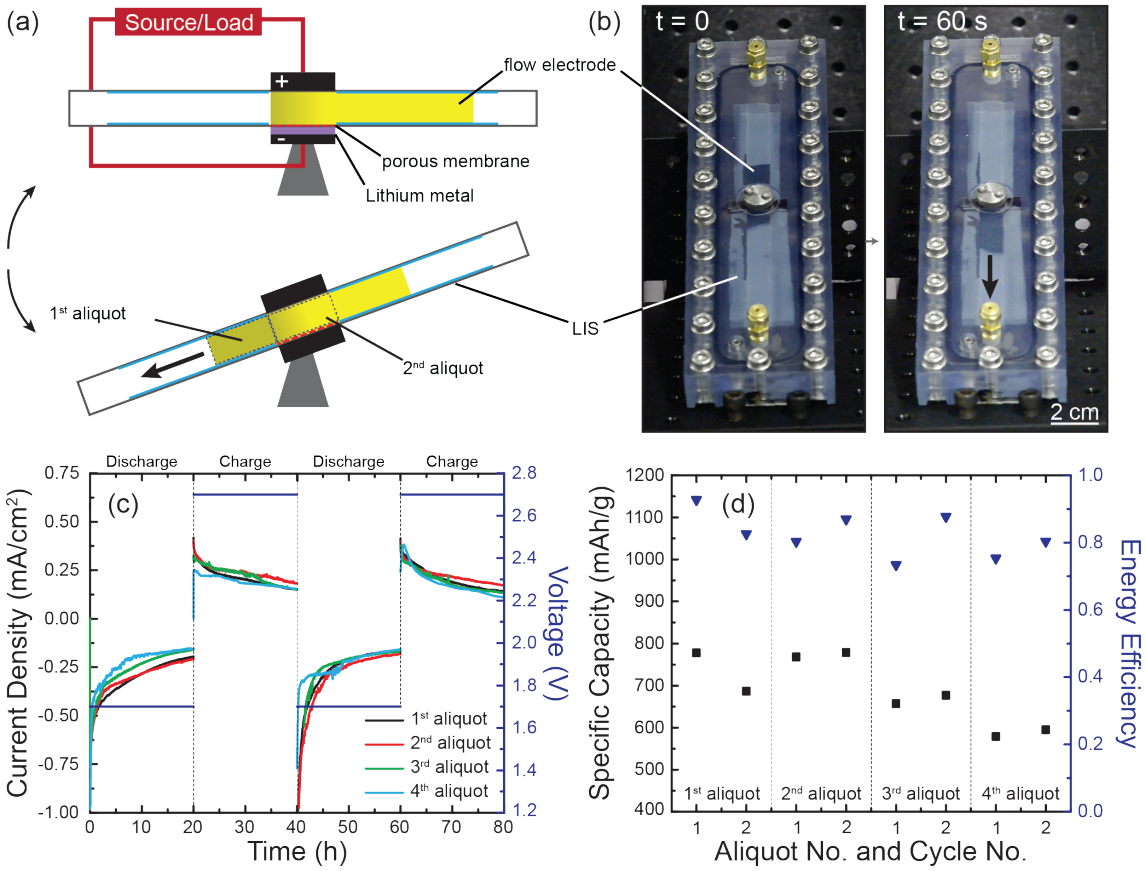

Figure 5: (a) Schematic of the GIFcell half-flow configuration with lithium metal as the anode and the Li-PS suspension as the flowable cathode. The GIFcell operates in intermittent flow mode where one aliquot moves into the electroactive zone (between the two current collectors) and remains to undergo electrochemical cycling. Then, the GIFcell is tilted to move the next aliquot into the zone to undergo the same cycling. The Li-PS suspension consists of 2.5 M (with respect to sulfur) of Li_2S_8, 0.75vol% KB, 0.5 M LiTFSI, and 1wt% $LiNO_3$. (b) Time-lapse photos of the Li-PS suspension flowing over the electrochemical stack in the GIFcell (Supporting Video S5) demonstrate that the Li-PS suspension can repeatedly flow on the LIS in the GIFcell. The first frame shows the the GIFCell immediately after being flipped, and the second frame shows 60 seconds later after the flow electrode has passed through the current collector. (c) Current density against time for the GIFcell during electrochemical cycling for four aliquots. Each aliquot was subjected to two potentiostatic cycles of discharging at 1.7 V for 20 h and charging at 2.7 V for 20 h. (d) The specific capacity of the GIFcell during discharge (black

squares) and the round-trip efficiency (blue triangles) of the GIFcell with LIS for the four aliquots where each aliquot is subjected to two electrochemical cycles.